ELSEVIER

Physica B 244 (1998) 15–21

PHYSICA B

Dynamical conductivity of an MBE-grown $La_{1.84}Sr_{0.16}CuO_4$ thin film at frequencies from 5 to 36 cm^{-1}

B.P. Gorshunov[a,*], A.V. Pronin[a], A.A. Volkov[a], H.S. Somal[b], D. van der Marel[b], B.J. Feenstra[b], Y. Jaccard[c,d], J.-P. Locquet[d]

[a] *General Physics Institute, Russian Academy of Sciences, Vavilov St. 38, 117942 Moscow, Russian Federation*
[b] *University of Groningen, Nijenborgh 4, NL-9747 AG Groningen, The Netherlands*
[c] *Institut de Physique, Université de Neuchâtel, CH-2000 Neuchâtel, Switzerland*
[d] *IBM Research Division, Zurich Research Laboratory, CH-8803 Rüschlikon, Switzerland*

Abstract

We present the first wide-band (5–400 cm^{-1}) measurements of the dynamical conductivity and the dielectric permittivity spectra of $La_{2-x}Sr_xCuO_4$ ($x \approx 0.16$). A narrow Drude-like band is observed in the spectra, which is consistent with a d-wave pairing state. We determine the plasma frequency, scattering rate, and mean free path of the unpaired charge carriers responsible for this band. For the first time, "coherence peak"-like behavior is observed in the temperature dependence of the submillimeter conductivity of $La_{2-x}Sr_xCuO_4$, associated with the temperature evolution of the band in the superconducting state. Published by Elsevier Science B.V.

Keywords: Submillimeter waves; Conductivity; Dielectric permittivity; LSCO; Superconductivity

In studying the nature of superconductivity in high-T_c cuprates, much effort has been directed towards obtaining information on the symmetry and value of the superconducting energy gap. Many recent experimental results indicate a strongly anisotropic gap function possibly arising from a d-wave pairing mechanism. A characteristic feature of the d-wave scenario, in which the value of the gap changes over the Fermi surface and has zeroes along certain directions, is the appearance below T_c of low-energy (millielectron volt range) absorption bands [1, 2]. Thus, the study of the low-energy electrodynamics of high-T_c superconductors is of great importance for distinguishing among various types of pairing mechanisms and for understanding the nature of the superconducting (SC) state. In $YBa_2Cu_3O_{7-\delta}$, the most popular and best-studied high-T_c compound, the application of several spectroscopic techniques has demonstrated the existence of such excitations in the dynamic conductivity spectra $\sigma(\omega)$ at terahertz frequencies [3–7]. A narrow Drude-like peak in $\sigma(\omega)$ has also been detected in the normal state of $La_{2-x}Sr_xCuO_4$ (LSCO) films [8] and single crystals [9–11]. However, normal incidence and grazing incidence reflection measurements do not provide reliable values of the optical constants of high-T_c superconductors below 40 cm^{-1}. As a consequence, details of the temperature–frequency behavior of the conductivity $\sigma(\omega)$ and the permittivity $\varepsilon'(\omega)$ of the cuprates at

* Corresponding author.

0921-4526/98/$19.00 Published by Elsevier Science B.V.
PII S0921-4526(97)00455-9

millimeter–submillimeter (MM–SBMM) wavelengths remain virtually unexplored.

In the present work, we study the low-frequency complex conductivity of LSCO by applying the backward-wave oscillator (BWO)-based measurement technique. This technique was designed for measurements in the frequency range $\omega/2\pi = 3$–$40\ cm^{-1}$ (energies 0.4–5 meV), and has already been applied to a great variety of conducting and nonconducting materials [12–15].

We have studied a $La_{1.84}Sr_{0.16}CuO_4$ thin film prepared on a custom-designed molecular-beam epitaxy system. The deposition method used is neither a codeposition method nor a layer-by-layer deposition but consists of a block-wise deposition of various elements to form the desired compound only during the deposition of the final block with a minimum of intermediary phases [16, 17]. For the undoped LSCO compound grown on $SrTiO_3$ (STO) the probable interfacial stacking sequence is SrO–TiO_2–LaO–CuO_2–LaO as observed for $La_2SrCu_2O_6$ films [18]; this would indicate an "ideal" sequential layer-by-layer deposition procedure of one monolayer of LaO, followed by one monolayer of CuO_2 and another monolayer of LaO, after which the entire sequence is repeated. Such a process sequence is far from optimal because, once the CuO_2 monolayer has been deposited, LSCO will start to form, leaving about half the deposited Cu-oxide layer as precipitates. Hence, the preferred block-by-block sequence consists of depositing two monolayers of LaO followed by one monolayer of CuO_2. The properties of such films deposited on (0 0 1) STO or (0 0 1) $SrLaAlO_4$, whether doped with strontium or oxygen, have been reported elsewhere: strontium-doped films were used to study the doping dependence of the penetration depth [19] and coherence length [20], whereas oxygen-doped films were used to demonstrate the electrochemical oxidation of c-axis films [21, 22] as well as local electrochemical lithography [23]. Moreover, a detailed account of the microstructural properties of these thin films has also been published [24].

The LSCO film studied here was grown at a substrate temperature of 750°C on an approximately 1 mm thick $SrLaAlO_4$ substrate with a Sr content of 0.16 and a total thickness of 59 nm. The structural properties of the film, illustrated in the θ–2θ diffraction spectra (Fig. 1), can be summarized as follows: (i) besides the substrate peaks indicated by "S", only (0 0 l) peaks related to a c-axis-oriented epitaxial film are observed (the additional peaks are due to "forbidden" substrate reflections); (ii) the c-axis value of the film corresponds to 1.3277 nm, which is significantly greater than the one found in bulk material for this composition due to an in-plane compressive epitaxial stress [24]; (iii) the inset is an enlargement of the intensity around the (0 0 s) peak and reveals finite-size oscillations characteristic of a thin film with a surface roughness not exceeding 1 to 2 unit cells. The temperature-dependent DC resistivity is shown in Fig. 2 and reveals: (i) a linear decrease of resistivity versus temperature with a RRR ($R_{300\,K}/R_{40\,K}$) of about 6.5; and (ii) a critical temperature T_c of 38.5 K with a transition width ΔT_c of 1.5 K. The critical temperature of this film is as high as that of the best bulk LSCO material [25].

The MM–SBMM spectrometer is described in detail in Refs. [12, 13] and utilizes BWOs as monochromatic frequency-tunable radiation sources. Experimentally, the transmission coefficient Tr and

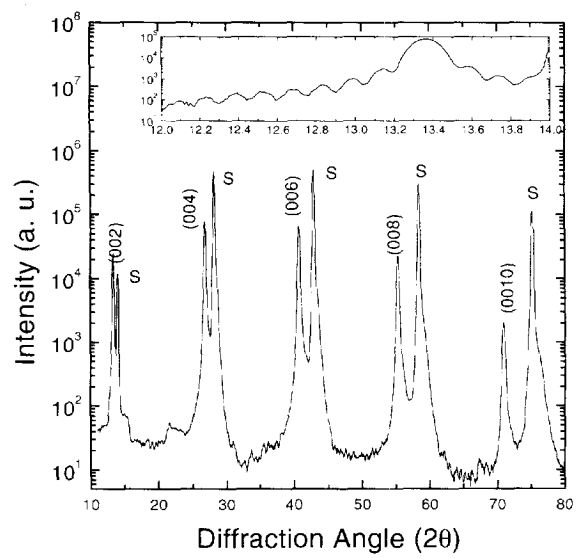

Fig. 1. X-ray diffraction spectrum of a LSCO film on $SrLaAlO_4$. Inset: finite-size oscillations around the (0 0 2) film peak.

the phase shift φ_t of the radiation transmitted through the plane-parallel substrate covered by the film are measured in a quasioptical arrangement. Spectra of both optical parameters of the film, conductivity $\sigma(\omega)$ and permittivity $\varepsilon'(\omega)$, are calculated *analytically* on the basis of general Fresnel expressions for $\mathrm{Tr}(\sigma, \varepsilon', \omega)$ and $\varphi_t(\sigma, \varepsilon', \omega)$ for the two-layered system (see Refs. [12, 13]), which take into account the dielectric parameters of the substrate n and k (refraction and extinction coefficients, respectively) and interference effects in the substrate. In our case the optical thickness nd of the substrate (thickness $d \approx 1$ mm, $n \approx 4$, see below) is greater than the radiation wavelength $\lambda \leqslant 1$ mm, so that the substrate serves as an asymmetrical Fabry–Pérot resonator, whose mirrors are its two faces, one with and one without the film. The transmission coefficient spectrum of such a system contains interference maxima, whose separation $\Delta\omega$ is determined to be $\Delta\omega \approx c(2nd)^{-1}$ and whose amplitudes depend mainly on the transmission coefficient of the LSCO film (because the extinction coefficient k of the substrate is $k \ll 1$, see below). At the frequencies corresponding to these maxima, the measured values of Tr and φ_t are most sensitive to the optical parameters of the film, thus, we analyze below the data at frequencies corresponding to transmission coefficient maxima of the interference pattern. In addition to SBMM measurements, we measured the far-infrared (FIR) reflectivity at a grazing angle of incidence with p-polarized light of a LSCO single crystal, from which we obtained the complex optical constants using Kramers–Kronig relations [9]. Together, these two types of measurements provide wide-band (5–400 cm^{-1}) spectra of $\sigma(\omega)$ and $\varepsilon'(\omega)$.

MM–SBMM measurements of the film were taken in the frequency range from 5 to 36 cm^{-1} at temperatures between 5 and 300 K. Before extracting the SBMM characteristics of the film, we first had to measure the dielectric parameters n and k of the substrate. These measurements were taken using a plane-parallel piece of the substrate, free of film. The "transmission coefficient" method [12, 13] was used, and n and k were calculated on the basis of the substrate transmission coefficient spectra. We found that at room temperature the value of n is $4.1 \pm 0.2\%$ and decreases by about 1%

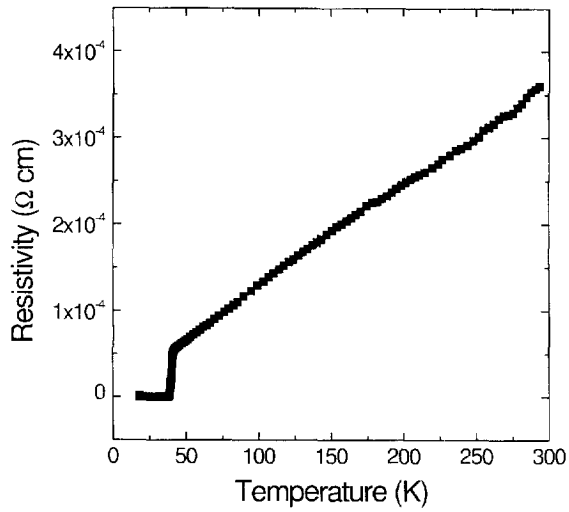

Fig. 2. Resistivity as a function of temperature of the LSCO film on $SrLaAlO_4$.

at liquid-helium temperature. At all temperatures, a slight increase of $k(\omega)$ towards high frequencies was found. For instance, at 300 K the value of k is about 10^{-3} at 10 cm^{-1} and increases approximately threefold at 30 cm^{-1}. Regarding the temperature dependence, k decreases slightly at lower temperatures.

To demonstrate the original SBMM data, we present in Fig. 3 typical transmission-coefficient and phase-shift spectra of the film/substrate system. The periodic oscillations in the spectra are due to multiple reflections of the radiation inside the plane-parallel dielectric substrate. Above T_c, the transmission coefficient maxima at a fixed temperature have equal amplitudes which decrease with decreasing temperature, indicating an increase of the normal-state conductivity of the film (and a corresponding decrease of its transmission coefficient). Strong changes occur in the spectra below T_c caused by the transition of the film into the SC state: a noticeable frequency dispersion appears in the $\mathrm{Tr}(\omega)$ spectrum and distinct knees are seen at T_c in the temperature dependence of Tr and φ_t (Fig. 4, upper panel). At the frequency 5.8 cm^{-1}, the value of Tr decreases at 5 K by about one order of magnitude compared with that at T_c, whereas this decrease is less pronounced at higher

frequencies. The magnitude of the phase shift remains approximately unchanged above T_c (Fig. 6) but decreases by more than 1 rad at liquid-helium temperature, with a tendency to decrease further at lower temperatures to the maximal phase shift of 90°, which is expected when the film goes from the normal to the SC state.

Fig. 5 illustrates the main experimental results of the present paper: the wide-band spectrum of the frequency dependence of the conductivity and dielectric permittivity of the LSCO film (SBMM spectra) and of the LSCO single crystal (grazing FIR reflectivity). An increase of the SBMM conductivity of the film with decreasing temperature below T_c is clearly seen. Above 30 cm^{-1} we see the opposite trend: $\sigma(\omega)$ is suppressed below the phase transition, in agreement with earlier data on films [8] and single crystals [9–11]. We observe that the present MM–SBMM data is even more indicative than earlier results of an incomplete suppression of $\sigma(\omega)$, in contrast to the behavior expected for isotropic s-wave superconductivity, but in agreement

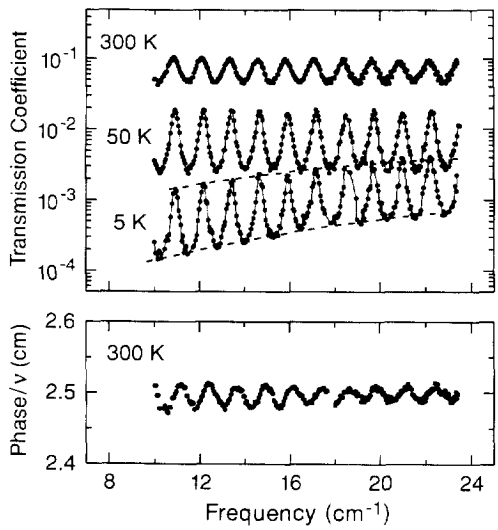

Fig. 3. Low-frequency fragment of submillimeter spectra of transmission coefficient and phase shift (divided by the frequency in wave numbers) of a LSCO film on a $SrLaAlO_4$ substrate. Dashed lines are guides to the eye.

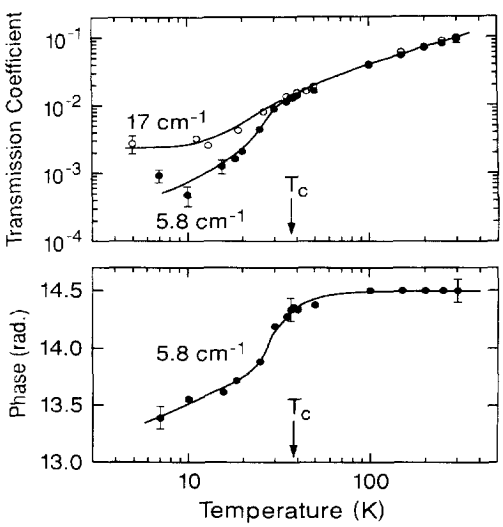

Fig. 4. Temperature dependences of SBMM transmission coefficient and phase shift of a LSCO film on a $SrLaAlO_4$ substrate at two frequencies.

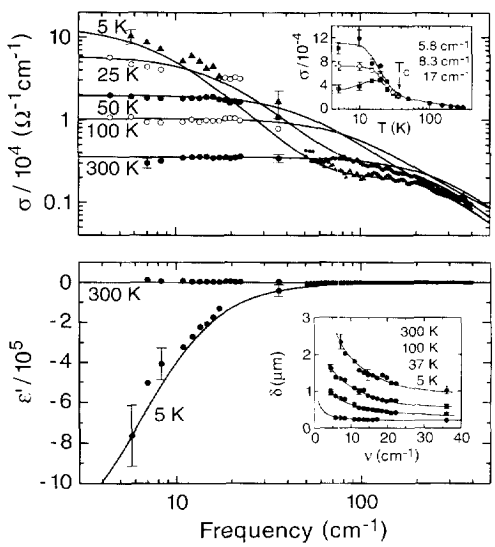

Fig. 5. Frequency dependences of conductivity and dielectric permittivity of LSCO at various temperatures. Solid lines are a least-squares fit by the model containing the Drude term, responsible for the SBMM part of the spectra, and the oscillator term, which describes the IR dispersion. Upper panel inset: temperature dependences of SBMM conductivity at three frequencies. Lines are guides to the eye. Lower panel inset: frequency dependences of the penetration depth $\delta = c(\kappa\omega)^{-1}$ calculated from $\sigma(\omega)$ and $\varepsilon'(\omega)$ spectra. Lines are guides to the eye; line for the 5 K spectrum is the result of the fit of the 5 K $\sigma(\omega)$ and $\varepsilon'(\omega)$ spectra.

with scenarios in which the gap has nodes at the Fermi surface. We note that the overall wide-band behavior of $\sigma(\omega)$ in LSCO is qualitatively the same as that observed for the YBCO compound [25]: there is a broad wing in $\sigma(\omega)$ at IR frequencies, on the background of which a narrow band develops quickly in the SBMM range below T_c. At high temperatures (above T_c), $\sigma(\omega)$ and $\varepsilon'(\omega)$ are frequency independent at low frequencies, whereas below T_c a decrease of $\sigma(\omega)$ and an increase of $\varepsilon'(\omega)$ towards higher frequencies is observed. This is characteristic of Drude behavior, which suggests that the response of LSCO below 30 cm^{-1} is due to unpaired charge carriers, an observation which motivates us to fit the SBMM spectra using the corresponding Drude expressions [26]:

$$\sigma(\omega) = \sigma_0[1 + (\omega/2\pi\gamma)^2]^{-1},$$
$$\varepsilon'(\omega) = \varepsilon_{inf} - 2\sigma_0\gamma^{-1}[1 + (\omega/2\pi\gamma)^2]^{-1}, \quad (1)$$

where σ_0 is the DC conductivity, γ the scattering rate, and ε_{inf} the high-frequency contribution to the permittivity. Noticeable dispersion of the low-frequency behavior of $\varepsilon'(\omega)$ and $\sigma(\omega)$ in the SC state allows us to determine γ, σ_0, and the plasma frequency ω_{pl}^n [26] of the uncondensed charge carriers by performing a least-squares fit (see Fig. 5)

$$\omega_{pl}^n/2\pi = (2\sigma_0\gamma)^{1/2} = 7800 \pm 1500\ cm^{-1}. \quad (2)$$

The plasma frequency of the SC condensate ω_{pl}^s can be determined by taking into account the dielectric contribution to the dielectric permittivity that stems from the zero-frequency-centered delta function. According to Ref. [27], this contribution is given by

$$\varepsilon_s' = -(\omega_{pl}^s/\omega)^2. \quad (3)$$

Considering the dispersion of the ε' measured spectra as a "mixture" of two contributions, one from the dispersion of the conductivity at SBMM wavelengths, the other from the delta function, and making a corresponding least-squares fitting analysis, we obtain an estimate of $\omega_{pl}^s/2\pi \approx 3900\ cm^{-1}$ at 5 K. The plasma frequency of the total number of carriers can then be determined as $\omega_{pl}^0/2\pi = \sqrt{(\omega_{pl}^s)^2 + (\omega_{pl}^n)^2}/2\pi \approx 8700 \pm 1500\ cm^{-1}$, which is close to the values determined in Ref. [28] (7020 cm^{-1}) and in Ref. [8] (6300 $\pm$ 100 cm^{-1}) and allows us to estimate the fraction of the condensed carrier density, $n^s/n^0 = (\omega_{pl}^s/\omega_{pl}^0)^2 \approx 20\%$, and the London penetration depth, $\lambda_L = c/\omega_{pl}^s \approx 0.4$ μm (c is the velocity of light). Our value of λ_L is in good agreement with the results of thin-film kinetic inductance [19], single-crystalline microwave (0.4 μm) [29], single-crystalline IR (0.43 μm) [9, 10], and polycrystalline μSR (0.3 μm) [30] measurements.

The dispersion of the SBMM $\varepsilon'(\omega)$ and $\sigma(\omega)$ disappears in the normal state, thus only the σ_0 parameter can be found from the dispersionless SBMM $\sigma(\omega)$ spectra. Taking the value of ω_{pl}^0 we can then use relation, Eq. (2), to calculate the scattering rate γ in the normal state. Fig. 6 shows the temperature dependences of the DC conductivity, the scattering rate, the mean free path $l = v_F/\gamma$ (with the Fermi velocity of $v_F \approx 2.2 \times 10^7$ cm/s taken from Ref. [28]) and the radiation penetration depth $\delta = c(\omega k)^{-1}$ (where k is the extinction coefficient of the film calculated from the measured values of ε' and σ) obtained with this procedure. No *sharp* anomalies in these quantities are observed at the critical temperature. The observed decrease of γ in the SC

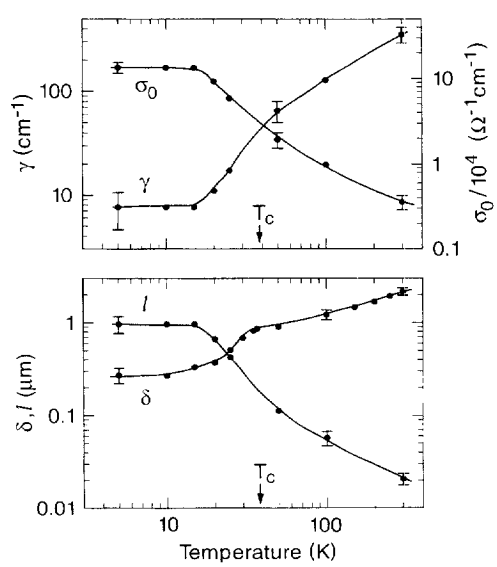

Fig. 6. Temperature dependences of the Drude model parameters (upper panel) obtained by a least-squares fit of the conductivity and permittivity spectra of the LSCO (Fig. 3) and the calculated mean free path $l = v_F/\gamma$ and radiation penetration depth $\delta = c(\kappa\omega)^{-1}$ (lower panel).

state is one order of magnitude weaker than that reported for the LSCO film in Ref. [8] and two orders of magnitude weaker than that for the Y-based compounds reported in Refs. [5, 7]. This decrease of the scattering rate (or of the half-width of the Drude band) leads to the "coherence peak"-like behavior of the conductivity as observed in the inset of the upper panel of Fig. 5.

As seen in Fig. 6, at all temperatures below T_c, the values of δ and l are much greater than the coherence length $\xi_0 \approx 1.0$ nm, confirming that the case of a clean limit and local regime is realized for the SC condensate. At 300 K the ratio $l/\delta \approx 0.01$ is much less than unity, meaning that the local approach holds. However, at liquid-helium temperatures the locality condition $l/\delta \ll 1$ for the normal component is violated, with the formal crossover from the local to the nonlocal regime at $T \approx 25$ K where $l = \delta$. This could lead to the inapplicability of all "local" expressions used for the treatment of our data. However, we emphasize the two-dimensional character of the charge carrier motion in LSCO. As mentioned in Ref. [7], this would secure the local type of their interaction with the electromagnetic field: moving parallel to the film surface between two consecutive scatterings, the charge carrier will not leave and re-enter the region where the external field penetrates.

As illustrated in Fig. 5, we did not detect the familiar spectroscopic features of conventional s-wave superconductivity, which are strongly pronounced in the conductivity and permittivity MM–SBMM spectra of conventional superconductors [13–15, 25, 31]. First, there is no decrease of the SBMM conductivity in the SC state, which might indicate an energy-gap opening. Instead, its *strong increase* in the range from 5 to 36 cm^{-1} is detected below T_c. Second, we do not clearly observe the "dielectric signature" of the zero-frequency conductivity delta function, which is responsible for the DC supercurrent. The dielectric response of such a delta function should manifest itself as a strong dispersion of the permittivity at the *finite* frequencies given by Eq. (3).

Actually, we *do* see a strong dispersion of $\varepsilon'(\omega)$ of that type (Fig. 5). However, as shown above, this behavior of $\varepsilon'(\omega)$ and the corresponding dispersionless penetration depth (see inset in lower panel of Fig. 5, 5 K curve) cannot be associated *exclusively* with the zero-frequency delta function because both are due, at least in part, to the high-frequency Drude response of the unpaired carriers.

In conclusion, we have performed the first wide-band (5–400 cm^{-1}) measurements of the conductivity and dielectric permittivity spectra of LSCO with an emphasis on the millimeter–submillimeter range between 5 and 36 cm^{-1}. A narrow Drude-like band is observed in the conductivity spectra, the half-width of which decreases to 8 cm^{-1} in the superconducting state. Microscopic characteristics of the unpaired charge carriers, which could be responsible for the origin of the band, are determined: the plasma frequency, the scattering rate, and the mean free path. Coherence-peak-like behavior is observed in the temperature dependence of the submillimeter conductivity, which is associated with the thermal evolution of the quasi-particle conductivity in the superconducting state.

This work was supported by the Russian Foundation for Basic Research (No. 96-02-17350) and by the Ministry of Science and Technology (Grant No. 3.2 Physics of Microwaves). The authors thank the Swiss National Science foundation for financial support through the PNR 30 program.

References

[1] J.P. Carbotte, C. Jiang, D.N. Basov, T. Timusk, Phys. Rev. B 51 (1995) 11 798.
[2] H. Yamagata, H. Fukuyama, J. Phys. Soc. Japan 65 (1996) 2204.
[3] A.A. Volkov, B.P. Gorshunov, G.V. Kozlov, S.I. Krasnosvobodtsev, E.V. Pechen, O.I. Sirotinskii, J. Petzelt, Sov. Phys. JETP 68 (1989) 148.
[4] M.C. Nuss, P.M. Mankievich, M.L. O'Malley, E.H. Westerwick, P.B. Littlewood, Phys. Rev. Lett. 66 (1991) 3305.
[5] R. Buhleirer, S.D. Brorson, I.E. Trofimov, J.O. White, H.-U. Habermeier, J. Kuhl, Phys. Rev. B 50 (1994) 9672.
[6] D.A. Bonn, S. Kamal, K. Zhang, R. Liang, D.J. Baar, E. Klein, W.N. Hardy, Phys. Rev. B 50 (1994) 4051.
[7] D.A. Bonn, R. Liang, T.M. Riseman, D.J. Baar, D.C. Morgan, K. Zhang, P. Dosanjih, T.L. Duty, A. MacFarlane, G.D. Morris, J.H. Brewer, W.N. Hardy, C. Kallin, A.J. Berlinksy, Phys. Rev. B 47 (1993) 11 314.
[8] F. Gao, D.B. Romero, D.B. Tanner, J. Talcachio, M.G. Forrester, Phys. Rev. B 47 (1993) 1036.

[9] H.S. Somal, B.J. Feenstra, J. Schutzmann, Jae Hoon Kim, Z.H. Barber, V.H.M. Duijn, N.T. Hien, A.A. Menovsky, M. Palumbo, D. van der Marel, Phys. Rev. Lett. 76 (1996) 1525.
[10] H.S. Somal, Ph.D. Thesis, University of Groningen, 1997, in preparation.
[11] S. Uchida, K. Tamasaku, K. Takenoka, Y. Fukuzumi, J. Low-Temp. Phys. 105 (1996) 723.
[12] A.A. Volkov, Yu.G. Goncharov, G.V. Kozlov, S.P. Lebedev, A.M. Prokhorov, Infrared Phys. 25 (1985) 369.
[13] G. Kozlov, A. Volkov, Coherent source submillimeter wave spectroscopy, in: G. Gruner (Ed.), Millimeter Wave Spectroscopy of Solids, Springer, Heidelberg, 1997, in press.
[14] B.P. Gorshunov, I.V. Fedorov, G.V. Kozlov, A.A. Volkov, A.D. Semenov, Solid State Commun. 87 (1993) 17.
[15] A.V. Pronin, B.P. Gorshunov, A.A. Volkov, G.V. Kozlov, N.P. Shabanova, S.I. Krasnosvobodtsev, V.S. Nozdrin, E.V. Pechen, Sov. Phys. JETP 82 (1996) 790.
[16] J.-P. Locquet, A. Catana, E. Mächler, C. Gerber, J.G. Bednorz, Appl. Phys. Lett. 64 (1994) 372.
[17] J.-P. Locquet, E. Mächler, MRS Bull. 19 (1994) 39.
[18] K. Verbist, O. Milat, G. Van Tendeloo, F. Arrouy, E.J. Williams, C. Rossel, E. Mächler, J.-P. Locquet, Phys. Rev. B, 1997, in press.
[19] J.-P. Locquet, Y. Jaccard, A. Cretton, E.J. Williams, F. Arrouy, E. Mächler, T. Schneider, Ø. Fischer, P. Martinoli, Phys. Rev. B 54 (1996) 7481.
[20] Y. Jaccard, T. Schneider, J.-P. Locquet, E.J. Williams, P. Martinoli, Ø. Fischer, Europhys. Lett. 34 (1996) 281.
[21] F. Arrouy, J.-P. Locquet, E.J. Williams, E. Mächler, R. Berger, Ch. Gerber, Ch. Monroux, J.-C. Grenier, A. Wattiaux, Phys. Rev. B 54 (1996) 7512.
[22] J.-P. Locquet, Ch. Gerber, A. Cretton, Y. Jaccard, E.J. Williams, E. Mächler, Appl. Phys. A 57 (1993) 211.
[23] J.-P. Locquet, F. Arrouy, E. Mächler, M. Despont, P. Bauer, E.J. Williams, Appl. Phys. Lett. 68 (1996) 1999.
[24] J.-P. Locquet, E.J. Williams, Acta Phys. Pol. A, 1997, in press.
[25] D.B. Tanner, T. Timusk, in: D.M. Ginsberg (Ed.), Physical Properties of High Temperature Superconductors, vol. 3, World Scientific, Singapore, 1992.
[26] A.V. Sokolov, Optical Properties of Metals, Elsevier, New York, 1967.
[27] M. Suzuki, Phys. Rev. B 39 (1989) 2312.
[28] P.B. Allen, W.E. Pickett, H. Kraukauer, Phys. Rev. B 36 (1987) 3926.
[29] T. Scibauchi, H. Kitano, K. Uchinokura, A. Maeda, T. Kimura, K. Kishio, Phys. Rev. Lett. 72 (1994) 2263.
[30] Y.J. Uemura, G.M. Luke, B.J. Sternleib, J.H. Brewer, J.F. Carolan, W.N. Hardy, R. Kadono, J.R. Kempton, R.F. Kiefl, S.R. Kreitzman, P. Mulhern, T.M. Riseman, D.L. Williams, B.X. Yang, S. Uchida, H. Takagi, J. Gopalakrishan, A.W. Sleight, M.A. Subramanian, C.L. Chien, M.Z. Cieplak, Gang Xiao, V.Y. Lee, B.W. Statt, C.E. Stronach, W.J. Kossler, X.H. Yu, Phys. Rev. Lett. 62 (1989) 2317.
[31] M. Tinkham, Introduction to Superconductivity, Krieger, New York, 1975.